



HAL
open science

Seismic tomography of Central São Miguel, Azores

Daria Zandomeneghi, Javier Almendros, Jesús M. Ibáñez, Gilberto Saccorotti

► **To cite this version:**

Daria Zandomeneghi, Javier Almendros, Jesús M. Ibáñez, Gilberto Saccorotti. Seismic tomography of Central São Miguel, Azores. *Physics of the Earth and Planetary Interiors*, 2008, 167 (1-2), pp.8. 10.1016/j.pepi.2008.02.005 . hal-00532136

HAL Id: hal-00532136

<https://hal.science/hal-00532136>

Submitted on 4 Nov 2010

HAL is a multi-disciplinary open access archive for the deposit and dissemination of scientific research documents, whether they are published or not. The documents may come from teaching and research institutions in France or abroad, or from public or private research centers.

L'archive ouverte pluridisciplinaire **HAL**, est destinée au dépôt et à la diffusion de documents scientifiques de niveau recherche, publiés ou non, émanant des établissements d'enseignement et de recherche français ou étrangers, des laboratoires publics ou privés.

Accepted Manuscript

Title: Seismic tomography of Central São Miguel, Azores

Authors: Daria Zandomeneghi, Javier Almendros, Jesús M. Ibáñez, Gilberto Saccorotti

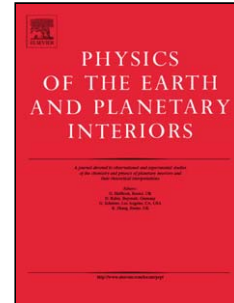
PII: S0031-9201(08)00028-9
DOI: doi:10.1016/j.pepi.2008.02.005
Reference: PEPI 4896

To appear in: *Physics of the Earth and Planetary Interiors*

Received date: 19-4-2007
Revised date: 14-11-2007
Accepted date: 4-2-2008

Please cite this article as: Zandomeneghi, D., Almendros, J., Ibáñez, J.M., Saccorotti, G., Seismic tomography of Central São Miguel, Azores, *Physics of the Earth and Planetary Interiors* (2007), doi:10.1016/j.pepi.2008.02.005

This is a PDF file of an unedited manuscript that has been accepted for publication. As a service to our customers we are providing this early version of the manuscript. The manuscript will undergo copyediting, typesetting, and review of the resulting proof before it is published in its final form. Please note that during the production process errors may be discovered which could affect the content, and all legal disclaimers that apply to the journal pertain.



Seismic tomography of Central São Miguel, Azores

Daria Zandomeneghi^{1,+}, Javier Almendros^{1,2}, Jesús M. Ibáñez^{1,2}, Gilberto Saccorotti^{3,*}

¹Instituto Andaluz de Geofísica, Universidad de Granada, Campus de Cartuja, 18071 Granada, Spain

²Departamento de Física Teórica y del Cosmos, Universidad de Granada, Campus de Fuentenueva, 18071 Granada, Spain

³Istituto Nazionale di Geofisica e Vulcanologia (INGV) - Osservatorio Vesuviano, Via Diocleziano 328, 80124 Napoli, Italy

⁺Now at New Mexico Tech - 801 Leroy Place, Socorro, NM 87801, USA

^{*}Now at INGV - Sez. di Pisa, Via U. della Faggiola 32, 56126 Pisa, Italy

Version November 14, 2007

Contact info:

Javier Almendros, Instituto Andaluz de Geofísica, Universidad de Granada,

Campus de Cartuja s/n, 18071 Granada, Spain, tel +34 958 249552,

fax +34 958 160907, email alm@iag.ugr.es

Abstract. We determine the three-dimensional distribution of P- and S-wave velocities for Central São Miguel Island (Azores, Portugal) by tomographic inversion of local earthquake arrival times. We use P- and S-phases from 289 earthquakes recorded by a network of 20 seismometers. The model shows good resolution in the shallowest 5-6 km, as illustrated by different resolution tests. There are several velocity anomalies, interpreted as pyroclastic deposits, intrusive bodies, geothermal fields, and the effects of tectonics. A low V_p zone marks Furnas caldera, probably evidencing volcanoclastic sediments with development of intense geothermal activity. Another low V_p zone extends in correspondence of the highly fractured area between Fogo and the north coast. Conversely, strong positive anomalies are found south of Fogo and northwest of Furnas. They are interpreted in terms of high-density deposits and remnants of a plutonic intrusion. These interpretations are supported by distribution of V_p/V_s , and are consistent with previous geological, geochemical, and geophysical data.

1. Introduction

The Archipelago of Azores consists of nine volcanic islands located at about 38°N-28°W, in the triple junction zone among the American, Eurasian and African plates. The largest island is São Miguel (Figure 1). The structure of São Miguel is characterized by fault systems mainly trending NW-SE and E-W. The most important volcanic complexes are located at the intersection of these tectonic lineaments (see *Cruz* [2003] and references therein). In central São Miguel, the main volcanic structures are those of Fogo and Furnas. Both are central volcanoes with a summit caldera and a dominantly trachytic composition. Furnas is the youngest volcano and consists of a steep-sided, 8 × 5 km caldera complex formed during several collapses [*Guest et al.*, 1999]. In the last 3000 years, most eruptions were phreato-magmatic and occurred with an average recurrence interval of 320 years [*Moore et al.*, 2001]. The Fogo volcanic edifice rises to an elevation of ~1000 m above sea level, and is composed by lava flows, domes and pyroclastic deposits over an older submarine lava basement. See for example *Guest et al.* [1999] for a detailed description of the geology of the area.

Although Central São Miguel volcanoes have not erupted since the 17th century, the area is restless. Geothermal manifestations are conspicuous and constitute one of the most important present day indication of volcanism. Geothermal exploration and research evidence two main active fields, in the Ribeira Grande-Fogo and Furnas regions. In these fields, local tectonics seem to control subsurface flow and the alignment of fumaroles and thermal springs [*Ferreira and Oskarsson*, 1999]. The most intense thermal activity coincides with an E-W tectonic lineament in Furnas and a NW-SE fault system in Fogo [*Cruz*,

2003]. At Ribeira Grande, the geothermal field is possibly connected to a reservoir between Fogo and the northern coast, hosted by highly fractured, pyroclastic rocks [Muecke *et al.*, 1974; Gandino *et al.*, 1985; Carvalho *et al.*, 2006]. The heat source, especially for deeper levels of the field, could be a regional heat anomaly [Silveira *et al.*, 2006; Ritsema and Allen, 2003]. At Furnas, the heat source is probably the plutonic remnants of the most recent volcanism below the center of the caldera, although there are no clear signs of direct magmatic contribution in the discharge composition [Cruz *et al.*, 1999].

To study the structure related to the volcanic activity of the island, several investigations have been carried out. Camacho *et al.* [1997] performed a gravimetric study of São Miguel Island to determine the density distribution in the first kilometers. At depths around 8 km, the areas around Fogo and Furnas show two density minima separated, in Congro zone, by a high density region that shows a NE-SW trend. It extends to shallow depths (still present at 1 km) and has been interpreted as an old basaltic shield or a partly solidified magmatic body. Montesinos *et al.* [1999] focused on the gravimetric low density anomaly of Furnas area. At shallow levels, this anomaly is interpreted as low-density silicic caldera infill, mainly due to collapse processes, and volcanic products from several eruptions which occurred after the formation of the main caldera from radial and concentric fractures. Deformation and GPS measurements performed at Central São Miguel have revealed a slight inflation of the Furnas area [Sigmundsson and Tryggvason, 1995]. An explanation refers to the presence of fluids within a deep hydrothermal system beneath the caldera, sealed by an impermeable zone and forced to growing pressures. At Fogo, GPS stations show displacements toward the caldera, indicating a slight deflation of the volcano [Jónsson *et al.*, 1999]. This deflation could be due to a pressure decrease

in the magma chamber, or to the extraction of water and steam by a nearby geothermal power plant.

In the last years, thousands of earthquakes have been annually recorded and located around São Miguel island by the regional seismic network. Their origin is mostly related to the approximately WNW-ESE fault systems dominating the regional tectonics [e.g. *Udias et al.*, 1976; *Madeira and Ribeiro*, 1990]. Central São Miguel is crossed by different fault systems, trending NW-SE and E-W, and constitutes one of the most active seismogenic regions in the Azores [e.g. *Gongora et al.*, 2004; *Escuer*, 2006]. This observation is compatible with the focal mechanisms calculated in the area [*Udias et al.*, 1976; *Bufoorn et al.*, 1988] and the strike-slip faulting observed in the bathymetry [*Lourenço et al.*, 1998].

The local seismic network evidences that a substantial number of the earthquakes are swarms of local, low-magnitude earthquakes located in the area between Fogo and Furnas (D. Silveira, personal communication). Although the tectonic control seems important, a recent work by *Luis* [2006] suggests that these swarms are not generated by a tectonic-driven mainshock/aftershock mechanism. The most likely explanation is that Central São Miguel earthquake swarms have a volcano-tectonic origin.

Inhabited volcanic areas, where even a small eruption could produce considerable losses, pose important problems in terms of hazards. This consideration motivated an European Union-sponsored project (named *e-Ruption*) intended to quantify the present-day seismicity of various quiescent volcanoes in populated regions [*Saccorotti et al.*, 2004]. One of the selected sites was Central São Miguel, where a seismic survey was carried out in April-July 2003. In this paper, seismic data recorded in that experiment are used to determine the three-dimensional (3D) velocity structure of the central region of São Miguel.

This work represents a first attempt to establish the relationship between seismic velocity distribution and volcanic structures in São Miguel Island.

2. Instruments and data

Between April 4 and July 15, 2003, a temporary network including short-period and broad-band instruments, as well as three small-aperture seismic antennas, was deployed in São Miguel [Saccorotti *et al.*, 2004] to expand and complete the permanent network operated by “Sistema de Vigilancia Sismologica dos Açores” (SIVISA). During this period, our instruments recorded more than one thousand earthquakes. Most of them were local earthquakes (Figure 2) characterized by S-P times smaller than a few seconds and with magnitude-durations lower than 2.5. The daily average was 5-10 earthquakes per day, except for a single swarm in April 26-27 when more than 160 earthquakes occurred in a few hours (Figure 3).

Our starting data set consisted of visually-picked arrival times for P and S phases associated with 426 earthquakes, recorded in a seismic network of 26 stations (Figure 1). They mostly had a time difference between arrivals of P and S waves smaller than 3 s, and were hence considered as local earthquakes.

3. Method

We chose the seismic tomography code of Benz *et al.* [1996] to calculate the 3D velocity structure of Central São Miguel. This method is particularly appropriate for the study of volcanic areas, usually characterized by sharp velocity heterogeneities that can strongly affect seismic wave propagation. The method uses the finite difference technique of Podvin and Lecomte [1991] (later modified by Tryggvason and Bergman [2006]) to calculate travel

times and allows for the simultaneous inversion of the 3D P-wave velocity structure and earthquake locations. For these reasons, it has been applied to investigate the interior of several volcanoes such as Redoubt [Benz *et al.*, 1996], Etna [Villaseñor *et al.*, 1998], Kilauea [Dawson *et al.*, 1999] and Vesuvio [Scarpa *et al.*, 2002], and calderas, for example Campi Flegrei [Zollo *et al.*, 2003].

3.1. Preliminary model

To apply this method to the São Miguel data, we need an initial guess for the velocity model of the region and preliminary earthquake locations. A preliminary 1D velocity model was obtained using the code *Velost* [Kissling *et al.*, 1994], that determines the velocity structure where calculated travel times best fit the observed phase arrivals, in a least-square sense. To calculate our 1D model, we started with the “Terra Açores” (TAC) velocity model used in routine network locations by SIVISA [Escuer, 2006] and with a selection of 331 earthquakes with good quality of recorded signals. We tested several layering thicknesses and more than 100 initial models differing a random 10% with respect to the TAC model. We obtained a 1D model which slightly differed from the TAC model, mostly in the first 5 km of depth (Figure 4). In the calculated 1D model, the RMS reduced from 0.044 to 0.018 s. The average displacement for the earthquake locations was 0.02 km and 0.07 km in horizontal and vertical direction respectively.

Preliminary hypocenter locations for 426 earthquakes in the whole São Miguel area were then obtained with the location algorithm *Nonlinloc* [Lomax *et al.*, 2000], which provides a maximum-likelihood solution for the source location problem. Arrival times were weighted according to their picking uncertainty. Quality levels of 0, 1, 2, 3, 4 were assigned respectively to time errors <0.02 , 0.02-0.05, 0.05-0.1, 0.1-0.2 and >0.2 s. We

found that most earthquakes are located in Central São Miguel, between Fogo and Furnas calderas, in the shallowest 10 km (Figure 5).

3.2. 3D Model

For the 3D velocity inversion, we selected 289 earthquakes with a minimum of 6 phase readings, a maximum station gap of 180° , a maximum offset between stations and earthquakes of 20 km, and a minimum distance between hypocenters of 0.4 km. A $20 \times 12 \times 11$ km volume centered at -25.426°W and 37.774°N , extending from 1.5 km above sea level to a depth of 9.5 km, was selected for the tomographic inversion. The final database consisted of 2197 P-wave and 1786 S-wave travel times, recorded at 20 stations (14 short-period and 6 broad-band seismometers) located within the selected area. Taking into account the station and hypocenter distributions, we estimate that the central region of São Miguel is densely sampled by seismic rays to a depth of 7 km. The volume was parameterized with a grid of constant-slowness cubic cells. After several tests with different cell sizes, we selected a 1-km cell as the optimum dimension for our inversion. It represented a good trade-off between travel time RMS, model resolution, and ray coverage [Benz *et al.*, 1996]. A denser grid of 0.25 km, obtained by linear interpolation of the 1 km grid, was used in the direct problem to calculate arrival times with an accurate ray path tracing. Figure 5 shows the area and inversion grid selected for the 3D tomography; the locations of the selected stations and hypocenters; and the ray path coverage.

The selection of the smoothing parameter was based on minimizing the final RMS without introducing instabilities or increasing the model roughness due to modelling of the noise [Benz *et al.*, 1996]. Moreover, we observed that low smoothing results in a decrease of the number of ray paths that the model was able to adjust. The best balance

between RMS and number of rays was achieved for a smoothing value of 60 (Figure 6). Convergence of the tomographic inversion to a stable solution was obtained after 10 iterations. Using the P and S travel time data and a V_p/V_s ratio of 1.68 derived for the same area [Saccorotti *et al.*, 2004; Escuer, 2006], the method provides relocated hypocenters and a 3D P-wave velocity model for Central São Miguel (hereafter, the CSM model).

The inversion code does not allow for variations of the V_p/V_s ratio across the model. Therefore, we used an indirect approach to obtain the 3D V_p/V_s distribution. We separated the source location and velocity determination problems and estimated independent velocity models for P- and S-wave velocities. We assumed that the hypocenters were fixed at the locations determined by our final, full-dataset inversion. To make comparable the resulting velocity models, we selected only those earthquakes with both P- and S-wave travel times. Then, we performed two independent inversions for velocity: (1) we used the P-wave travel times to obtain the P-wave velocity model; and (2) we used the S-wave travel times as first arrivals for the S-wave velocity model. The initial S-wave model is derived from the starting 1D velocity model for the P-wave and a V_p/V_s of 1.68. The V_p/V_s model is calculated as the ratio between the obtained P and S velocity models.

3.3. Resolution tests

The influence of systematic and random errors on the final results is hard to quantify owing to the nonlinear nature of seismic tomography, the difficulty of quantifying noise in the input data, and the effect of parameterization [Leveque *et al.*, 1993; Calvert *et al.*, 2000]. A number of empirical methods of uncertainty estimation are used to ensure that only robust, well-constrained features of the final model are interpreted. They are based

on the definition of artificial models with known distribution, dimension, and intensity of anomalies. The procedure presents two steps: first we solve the direct problem to determine synthetic travel times and then we use those data as input for the inverse problem. The source-receiver geometry and inversion parameters have to be as close as possible to those used for the real data. The comparison of the final model with the initial (known) model provides a qualitative indication about the resolving capabilities. Regions where the recovered model closely matches the input model are considered well resolved. However, the degree of recovery is sensitive to the geometry and magnitude of the synthetic anomalies. These factors also have to be considered when interpreting the tests.

We defined synthetic models to perform checkerboard tests [*Humphreys and Clayton, 1988*] and impulse response tests [*Ohmi and Lees, 1995*]. We also used the final velocity model to carry out a reconstruction test [*Zhao et al., 1992; Barberi et al., 2004*].

We built a checkerboard model characterized by alternated positive and negative anomalies of $\pm 10\%$ with respect to the initial 1D velocity model previously obtained. The anomaly dimensions were $3 \times 3 \times 4$ km. In this model, with the same configuration of earthquakes and stations as in the real inversion, we calculated synthetic travel times. The 1D initial model was then used as starting velocity structure for the inversion of the synthetic database. In Figure 7 we show results of the checkerboard test for a layer at 4 km depth and a E-W section at 1 km north of the center of the model. The best resolved areas are located in the center of the domain, to a depth of 5-6 km, in correspondence with largest ray path lengths and densely crisscrossed grid cells. Although the anomaly pattern is well reproduced, the intensity is generally underestimated.

As the geometry of the checkerboard anomalies is very different with respect to the final velocity model, and the seismic ray paths as well, we figured out the resolution also in other anomaly distributions.

For the impulse response tests, we generated smoothed spot-like anomalies at different locations in the domain. These anomalies are well reproduced in the final models, specially those with high velocities. The resolved volume again coincides with the high-coverage area (Figure 5), as in the checkerboard tests.

As an additional test, we calculated travel times in a velocity model equivalent to the CSM model. With this analysis we are able to check how well the inversion performs using anomalies with dimensions and positions similar to what we expect to deal with in the real medium. The parameter selection and inversion scheme was the same as in our 3D inversion. We added noise to the synthetic travel times in order to simulate the uncertainties in the real arrival time data. The noise level was inversely proportional to the quality assigned to the arrival time picks. To obtain a statistically robust estimate, this procedure was repeated to generate 25 noisy travel time data sets. When inverted, they generated a set of output models that show very slight differences among them. To compare the models, we used slowness rather than velocity because it shows a clearer Gaussian distribution of the final results. The standard deviations of slowness for each node are quite small, ranging between $1.1 \cdot 10^{-3}$ s/km and $8.7 \cdot 10^{-3}$ s/km, with a mean value of $5.1 \cdot 10^{-3}$ s/km. In Figure 8, we compare the average reconstructed model and our final CSM model. We observe that the main features are well recovered, as in previous test, until a depth of 5-6 km.

3.4. Input data tests

We assess the effects of the starting model and database characteristics. First, we performed the inversion using different trial structures as initial models. We perturbed the minimum 1D model by $\pm 10\%$ [Barberi *et al.*, 2004], and calculated the corresponding P-wave velocity structures. The results of this test indicate that positions and shapes of the anomalies do not significantly change inside the studied volume.

Next, we analyzed the control exerted on results by the database selection. We used a variation of the classical jackknife test, as suggested by [Lees and Crosson, 1989]. A strong advantage of this method is that it does not require an estimate of noise in the data to assess the uncertainty in the resulting model because the noise itself contributes to the variance in the derived models. We performed 25 different inversions, removing a random 10% of the initial dataset, and then examining the variance of the derived models. The standard deviations among these models could be assumed as a measure of the uncertainty in the final model. Standard deviations for slowness among the final models were calculated at each node. They ranged from $0.2 \cdot 10^{-3}$ s/km to $2.6 \cdot 10^{-3}$ s/km, with a spatially-averaged value around $1.1 \cdot 10^{-3}$ s/km. Comparing the average velocity model with the CSM model, we observe that the strongest differences occur at a few isolated points and are smaller than 6% of the averaged slowness at the same locations. From this point of view, the general framework of anomalies is not affected and main perturbations have a robust feature.

4. Results

Travel time data obtained during the 2003 experiment at São Miguel were inverted using the method described above. For P phase arrival times, the average residual between observed and calculated values in the minimum 1D model was 0.35 s; in the final 3D model it was reduced to 0.13 s. For the S phase the RMS reduction was from 0.44 to 0.15 s. This latter value refers to the inversion for the velocity model only. Earthquake locations changed an average of 0.09, 0.29, 0.25 km toward E, S, and depth. The origin times changed an average of 0.026 s.

The CSM model obtained contains several anomalous regions characterized by seismic velocities which differ from the starting values up to $\sim 10\%$. Figure 9 shows the distribution of V_p and V_p/V_s in Central São Miguel. Those zones poorly resolved by the inversion, due to insufficient coverage, are shaded in grey. Several remarkable features appear in the seismic structure. We image a low-velocity anomaly in the Furnas zone, highly stable down to 6 km depth. The velocity values are over 10% lower than those of the starting model. Another zone of low velocity is situated in the NW corner of the studied area, between Fogo caldera and the north coast. This negative anomaly is weaker than the SE anomaly, and never surpasses the 2-3% value. Moreover, it stands in a peripheral region of our volume and for this reason it is pointed out by our resolution tests as tentative. This has to be taken into account in the interpretation step. On the contrary, the region extending from the south of Fogo to the northwest of Furnas, across the Congro area, shows clear positive anomalies, around 10% in their strongest values. This anomaly is actually constituted by two volumes, in the NE and SW extremes, separated by a slower

zone. This zone has the highest ray coverage and thus this partition in two sub-regions is probably a real feature of the velocity structure.

For the vertical distribution of heterogeneities, we observe that the overall positions of the model contrasts do not strongly vary with depth. The main anomalies stand in their positions, slightly changing in intensity. This means that whatever mechanisms produce the velocity variations, they extend all the way down to the depth resolved by our inversion. Figure 10 shows interpolated vertical sections along two profiles (see Figure 9) across the main anomalies. In this figure, we show the deep, poorly resolved levels as well, in order to understand the likely vertical extent of the anomalies. For example, the Furnas low-velocity anomaly extends in depth from 1 to 5 km, while the Ribeira Grande anomaly appears to be deeper. On the other hand, the northeastern high-velocity region deepens more than the southwestern high-velocity.

With respect to the V_p/V_s ratio of 1.68 previously derived for this area, both higher and lower values are retrieved by our inversion (Figure 9). A central, high ratio volume stands in the whole depth range. Between 1 and 5 km depth, high values extend eastward, closer to the Furnas area. Slightly high ratios appear between Fogo and the south coast. Low V_p/V_s can be observed in the north-northwest part of our volume and in the Furnas caldera zone. The lowest V_p/V_s ratios in both regions are found at about 2 km depth.

The V_p and V_p/V_s distributions contain features that do not overlap. For example, the SW and NE high velocity anomalies imaged in the V_p structure have completely different behavior in terms of V_p/V_s . The NE area has a low V_p/V_s ratio, while the SW region has a slightly high value around 1.7-1.8. This is an indication that these two anomalies

are not related to the same processes, and underlines the need for V_p/V_s analysis when performing seismic tomography.

5. Discussion

From a seismological point of view, volcanic areas are complex structures. They exhibit solidified intrusions, partially molten regions, geothermally altered rocks, and intricate deposits of different shapes, thicknesses, and compositions. Therefore, volcanic regions are prone to enclose rocks with a wide range of physical properties [Foulger and Arnott, 1993]. In seismological terms, this variability translates into the occurrence of strong contrasts of seismic wave velocity. The scenario is further complicated by the presence of fluids and structural discontinuities, definitely common in volcanic environments. Such factors usually affect V_p and V_s in different ways. Typically, the spatial variation of V_p mirrors the distribution of lithologies and rock properties, while the V_p/V_s ratio maps rock defects, pores, cracks, and their fluid content [Berge and Bonner, 2002]. Since V_p and V_p/V_s are affected by different phenomena, both distributions have to be combined to envisage a global seismic structure.

During the last decades, a wealth of studies has demonstrated that seismic tomography is a useful technique to investigate the structures of volcanic regions. Low-velocity anomalies interpreted as partially molten volumes have been found at Toba Caldera [Masturyono *et al.*, 2001], Yellowstone [Husen *et al.*, 2004], and Rabaul [Finlayson *et al.*, 2003]. Low-velocity regions have also been associated with geothermal systems (e.g. Coso geothermal system [Wu and Lees, 1999; Sanders *et al.*, 1995], and low-density caldera infilling materials (e.g. Taupo volcanic zone [Sherburn *et al.*, 2003]). On the other hand, high-velocity

regions in volcanic areas are generally understood in terms of intrusive solidified volumes (e.g. Taupo volcanic zone [Sherburn *et al.*, 2003], Tunghuraua volcano [Molina *et al.*, 2005], and Bandai volcano [Yamawaki *et al.*, 2004]). The interpretation of V_p/V_s distributions has been addressed by several empirical and theoretical studies [e.g. Mavko, 1980; Dvorkin *et al.*, 1999; Wang *et al.*, 1998; Takei, 2002]. The variations of V_p/V_s with pressure, temperature, composition, porosity, etc, are difficult to model. For example, both decrease and increase of V_p/V_s have been observed after a change in confining pressure, depending on depth range, presence of microcracks, fluid contents, and thermal perturbations [Nicholson and Simpson, 1985; Bonner *et al.*, 1998; Patané *et al.*, 2002]. In spite of that, in volcanic environments high V_p/V_s values at shallow depths can be generally associated with saturated highly fractured materials (as in Vesuvio [Scarpa *et al.*, 2002] and Kilauea [Hansen *et al.*, 2004]). Deep, high V_p/V_s values are rather related to bodies of partial melt (as in Etna [Patané *et al.*, 2006], Yellowstone [Husen *et al.*, 2004] and Long Valley [Sanders *et al.*, 1995]). Low ratios can be also found in geothermal systems near the water-steam transition as in Yellowstone [Chatterjee *et al.*, 1985] and Onikobe volcanic area [Nakajima and Hasegawa, 2003].

In any case, the interpretation of V_p and V_p/V_s anomalies in terms of rock properties and geological structures is generally not unique. In order to narrow down the possible interpretations and correctly understand the tomographic results, we must take into account any information available from other geological, geochemical and geophysical studies.

5.1. Interpretation of velocity anomalies

To understand the nature and meaning of the velocity anomalies depicted in Figure 9, we are going to combine the information from the V_p and V_p/V_s models, and discuss them in the light of the results of previous studies about this region.

In the final results, the V_p distribution displays areas with low and high velocities, related to important lateral heterogeneities across Central São Miguel. We have revealed two low-velocity regions around Furnas and northwest of Fogo, as well as two high-velocity regions south of Fogo and northwest of Furnas. These high-velocity anomalies might be linked through a lower velocity region.

Regarding the V_p/V_s distribution, we find two areas of low V_p/V_s ratio around Furnas and north and northeast of Fogo. A region of normal or slightly high ratio occupies the center and southwest areas (Figure 9). In average, the V_p/V_s ratio in Central São Miguel tends to be low. The V_p/V_s ratio observed in active geothermal areas depends on the rock matrix, porosity, pore fluid content, pore pressure, temperature, and pore shape [Takei, 2002]. A low V_p/V_s ratio is thought to be caused by abundance of fractures filled with boiling water. In fact, the mechanism of water-steam transition has a stronger effect on compressibility than shear modulus, leading to low V_p/V_s ratios. The relationship between low V_p/V_s ratios and geothermal areas is so sound that the study of the V_p/V_s ratio was suggested as a promising technique to identify geothermal resources and monitor their exploitation [Julian *et al.*, 1996]. Contrarily, melt inclusions reduce S-wave velocity more than P-wave velocity, resulting in high V_p/V_s ratios. Therefore, the observation of low V_p/V_s values in Central São Miguel suggests that large volumes of partial melt are not present, at least within the shallowest crust.

The seismic study by *Dawson et al.* [1985] estimated an average V_p/V_s value of 1.53 to 1.62. It is interesting to note that this value is much lower than what we find in our V_p/V_s tomography or in the preliminary work on the *e-Ruption* data by *Saccorotti et al.* [2004]. Although the data base and instruments are quite different, we suspect that the reduction of the V_p/V_s ratio can be a real feature. We think that the difference could be attributed to the power plant production. The continuous exploitation of the geothermal system since the 80s could have decreased the steam fraction and/or cooled the system. This could be also the origin of the observed decrease of fumarolic activity [*Cruz, 2003*], and general deflation of the zone [*Jónsson et al., 1999*].

5.1.1. Low velocity regions

The low velocity regions around Furnas caldera and north of Fogo volcano share a set of characteristics. Basically, they are characterized by low P-wave velocities and low V_p/V_s ratios, which decrease with depth until they reach a minimum at ~ 2 km below sea level. Indications of low velocity in Furnas region comes also from the seismic profile of *Senos and Costa-Nunes* [1979]. They found a perturbation in the 2D velocity distribution indicating lower velocities below Furnas caldera. Results from gravity inversions [*Camacho et al., 1997; Montesinos et al., 1999*] indicate the presence of low-density bodies that coincide spatially with our low-velocity regions. Similar low-gravity anomalies have been related with low-density products of explosive volcanic activity and collapse processes by *Sherburn et al.* [2003] for Taupo zone calderas and *Vanorio et al.* [2005] for Campi Flegrei. Taking into account the mainly trachytic, explosive eruptive history of Fogo and Furnas volcanoes, the low-velocity anomalies may be attributed to the presence of pyroclastic products infilling the surrounding areas. These products include pumices, ignimbrite

and surge deposits, phreatomagmatic ashes, and dome materials [Guest *et al.*, 1999]. However, while this explanation can be referred to the shallow layers, the continuation of the anomalies in depth may be associated with intensely fractured and/or hydrothermally altered areas [Sanders *et al.*, 1995].

The V_p/V_s ratios are low for both of these areas. These values point to the presence of extensive steam-dominated geothermal fields. The variations of the velocity ratio with depth could be explained by changes in the fluid conditions. In the shallow part, water seems to dominate the reservoirs, producing a slightly higher V_p/V_s ratio. The existence of thermal springs near Furnas Lake points to a shallow, liquid-dominated geothermal field, which is consistent with the higher V_p/V_s ratio observed in the first layers. The deuterium-oxygen isotope signatures indicate that the dominant fluid most likely derives from down-flow meteoric water input [Ferreira and Oskarsson, 1999]. At larger depths, the sealed geothermal reservoir [Sigmundsson and Tryggvason, 1995] would be filled with fluid at supercritical conditions, yielding a lower V_p and V_p/V_s ratio. This decrease in V_p/V_s ratio with depth might suggest that the fluid become steam-dominated at depths around 2 km, closer to the heat sources. The existence of vapor-filled systems at depths of about 4 km has been directly observed in wells at several geothermal fields, for example The Geysers [Moore *et al.*, 2001].

Therefore, a geothermal system embedded in porous, low-density pyroclastic deposits could be the origin of the low V_p , low V_p/V_s , and low density values reported in these areas. Although the similarities point to a common explanation for the velocity anomalies in these areas around Furnas and Fogo, there are also a few differences. For example, the low velocity area north of Fogo is much weaker. The coverage, and therefore the resolution

capabilities of the tomography method, are low in this area. This can be at the origin of an underestimate of anomaly intensity.

Given this extensive geothermal activity, small amplitude, long-period seismicity of hydrothermal origin is likely to occur in Central São Miguel. In the area, long-period events and volcanic tremor, produced by the resonance of fluid-filled cavities within the volcanic medium [Chouet, 1996], have not been reported so far. The lack of noticeable volumetric, fluid-related seismic sources in Central São Miguel indicates that massive magma transport is not occurring. Nevertheless, such seismic activity might be difficult to detect without specialized instrumentation (i.e. seismic antennas) and/or adequate coverage near the geothermal areas. Recent improvement of instrumentation, with the deployment of a small aperture seismic array in the zone of Congro (A. Montalvo, personal communication), is expected to return interesting information about this kind of long-period seismic activity.

5.1.2. High velocity regions

The high velocity regions in Figure 9 are distributed along a NE-SW trend, from the south of Fogo to the northwest of Furnas. These anomalies could reflect the existence, at various depths, of welded thick pyroclastic deposits, domes and more compacted material. The NE-SW trend is compatible with the direction of normal faults in the area, either inferred [Carvalho *et al.*, 2006] or detected as electric discontinuities [Gandino *et al.*, 1985].

The Fogo volcano could stand as a chilled remnant of a magma chamber, as described, for example, by Dawson *et al.* [1985]. The absence of melt under the Fogo edifice is confirmed by the lack of evidence of magmatic activity from geophysical and geochemical surveys [Cruz *et al.*, 2006]. For example there is a general subsidence in the area [Jónsson

et al., 1999] and a decrease of the fumarolic system intensity [Cruz, 2003]. Moreover, the magmatic input of fumarolic system is considered not as strong as to justify a direct connection between hydrothermal and magmatic activity (*eRruption Working Group* [2004], and references therein).

We observe different V_p/V_s values for the two high velocity regions. V_p/V_s span the whole range between 1.8 (in the SW high V_p anomaly) and 1.65 (in the NE high V_p). They are likely due to different phenomena and constitute an excellent example of the importance of V_p/V_s ratio to interpret information by V_p distribution. The positive V_p anomaly located in Fogo area has a high V_p/V_s ratio. This could indicate that this intrusive part is marked by low V_s , i.e. fluids contained in fractures of the medium. From this point of view, we are imaging zones of transport, advection and crystallization of fluids through a solidified intrusive. Given the strong high- V_p anomaly, we think that water could be the fluid involved rather than melt. We guess that this fracture system represents the preferred path for up-welling of water toward the superficial geothermal fields. Something similar has been observed and explained with the presence of melt/water-saturated pathways in Etna volcano [Patané *et al.*, 2006] and Nevado del Ruiz [Londoño and Sudo, 2002]. On the other hand, the lower V_p/V_s ratio of the northeast high V_p anomaly could be due to cold volcanic material relatively unaffected by fracturing and geothermal circulation.

An intermediate region divides the two high V_p anomalies. This zone constitutes the main seismogenic region in Central São Miguel. Most of the relocated seismicity clusters here and shows a preferred NW-SE alignment [Bonagura *et al.*, 2004; Luis, 2006]. This direction dominates the tectonics of the zone also in surface geology [Guest *et al.*, 1999;

Gandino et al., 1985]. Although the constituent materials could be the same as in the neighbouring high V_p areas, the high crack density typical of faulted volumes would be at the origin of the observed lower velocity.

6. Conclusions

Our study represents a first attempt toward delineating and interpreting the subsurface seismic velocity structure of São Miguel Island. In the zone we are able to resolve, the velocity model depicts a complex picture of heterogeneities in which both V_p and V_p/V_s have large lateral contrasts over scale lengths of a few kilometres. Taking into account additional information from geophysical, geological and geochemical studies, we suggest an interpretation for the seismic velocity distribution in terms of volcanic structure. We identify pyroclastic deposits, intrusive bodies, geothermal fields, and the effects of tectonics.

In particular, we observe evidences of a vigorous geothermal field in Furnas, but not at Fogo caldera. In Fogo, everything points to the existence of the chilled remnant of a magmatic chamber, which nowadays constitutes only the pathway for water fluids. We do not find grounds for the existence of bodies of partial melt in the shallow structure.

We expect that this 3D velocity model will improve understanding of the past and present volcanic activity in Central São Miguel and the nature of the recorded seismicity. Moreover, this image could be of interest in risk evaluation and assessment for the densely inhabited areas of São Miguel.

As natural, more questions arise from the results of this seismic velocity tomography, mostly related with areas of low resolution and scale of resolved anomalies. Imaged

structures could be better depicted by a wider database. At this point, long-term data from a permanent seismic network would be desirable.

Acknowledgments. We thank Dr. Helffrich and two anonymous reviewers for their useful comments. The seismic survey was funded by the European Union project *e-Ruption* (EVR1-CT-2001-40021). Partial support also came from the projects ANT2001-3833, CLG2004-05744-C04-01 and CGL2005-05789-C03-02/ANT of the Spanish Ministry of Education, and from the European Union project *VOLUME* (FPG2004-GLOBAL-3-018471). We would like to acknowledge the effort and tireless fight against the elements of all participants in the field operations at São Miguel. We are especially indebted to Dr. Nicolau Wallenstein and his team, who managed the logistics and worked hard to keep the experiment going.

References

- Barberi, G., Cosentino, M. T., Gervasi, A., Guerra, I., Neri, G., Orecchio, B. (2004), Crustal seismic tomography in the Calabrian Arc region, South Italy, *Phys. Earth Planet. Int.*, 147, 297–314.
- Benz, H. M., Chouet, B., Dawson, P., Lahr, J., Page, R., Hole, J. (1996), Three-dimensional P and S wave velocity structure of Redoubt Volcano, Alaska, *J. Geophys. Res.*, 101, 8111–8128.
- Berge, P. A., Bonner, B. P. (2002), Seismic velocities contain information about depth, lithology, fluid content and microstructure, in *Symposium on the Application of Geophysics to Engineering and Environmental Problems*, pp. UCRL–JC–144792.

- Bonagura, M. T., Damiano, N., Saccorotti, G., Ventura, G., Vilardo, G., Wallenstein, N. (2004), Fault geometries from the space distribution of earthquakes at São Miguel, *Geophysical Research Abstracts*, 6, 07635.
- Bonner, B., Roberts, J., Duba, A., Kasameyer, P. (1998), Laboratory studies of Geysers rock, and impacts on exploration, *Geothermal Annual Program Review for DOE*.
- Bufo, E., Udías, A., Colombás, M. A. (1988), Seismicity, source mechanisms and tectonics of the Azores-Gibraltar plate boundary, *Tectonophysics*, 152, 89–118.
- Calvert, A., Sandvol, E., Seber, D., Barazangi, M., Roecker, S., Mourabit, T., Vidal, F., Alguacil, G., Jabour, N. (2000), Geodynamic evolution of the lithosphere and upper mantle beneath the Alboran region of the Western Mediterranean: Constraints from travel time tomography, *J. Geophys. Res.*, 105, 10871–10898.
- Camacho, A. G., Montesinos, F. G., Vieira, R. (1997), A three-dimensional gravity inversion applied to São Miguel, Azores, *J. Geophys. Res.*, 102, 7705–7715.
- Carvalho, M. R., Forjaz, V. H., Almeida, C. (2006), Chemical composition of deep hydrothermal fluids in the Ribeira Grande geothermal field (São Miguel, Azores), *J. Volcan. Geotherm. Res.*, 156, 116–134.
- Chatterjee, S. N., Pitt, A. M., Iyer, H. M. (1985), V_p/V_s ratios in the Yellowstone National Park region, Wyoming, *J. Volcan. Geotherm. Res.*, 26, 213–230.
- Chouet, B. (1996), Long period seismicity: its source and use in eruption forecasting, *Nature*, 380, 309–316.
- Cruz, J. V. (2003), Groundwater and volcanoes: examples from the Azores archipelago, *Environmental Geology*, 44, 343–355.

- Cruz, J. V., Coutinho, R. M., Carvalho, M. R., Oskarsson, N., Gislason, S. R. (1999), Chemistry of waters from Furnas volcano, São Miguel, Azores: fluxes of volcanic carbon dioxide and leached material, *J. Volcan. Geotherm. Res.*, 92, 151–167.
- Cruz, J. V., Antunes, P., Amaral, C., Franca, Z., Nunes, J. C. (2006), Volcanic lakes of the Azores archipelago (Portugal: Geological setting and geochemical characterization), *Mar. Geophys. Res.*, 20, 171–182.
- Dawson, P. B., da Silva, A. R., Iyer, H. M., Evans, R. (1985), Seismic study of the Agua de Pau geothermal prospect, São Miguel, Azores, *Geotherm. Res. Counc. Trans.*, 9(2), 401–406.
- Dawson, P. B., Chouet, B. A., Okubo, P. G., Villaseñor, A., Benz, H. M. (1999), Three-dimensional velocity structure of the Kilauea caldera, Hawaii, *Geophys. Res. Lett.*, 26(18), 2805–2808.
- Dvorkin, J., Mavko, G., Nur, A. (1999), Overpressure detection from compressional and shear-wave data, *Geophys. Res. Lett.*, 26, 3417–3420.
- eRruption Working Group (2004), Volcanic geology of São Miguel Island, *eRruption D 3.2.2.1 report, Geological Data*.
- Escuer, M. (2006), Improving seismic Vp and Vs models of the Azores archipelago.
- Ferreira, T., Oskarsson, N. (1999), Chemistry and isotopic composition of fumarole discharges of Furnas caldera, *J. Volcan. Geotherm. Res.*, 92, 169–179.
- Finlayson, D. M., Gudmundsson, O., Itikarai, I., Nishimura, Y., Shimamura, H. (2003), Rabaul volcano, Papua New Guinea: seismic tomographic imaging of an active caldera, *J. Volcan. Geotherm. Res.*, 124, 153–171.

- Foulger, G. R., Arnott, S. K. (1993), *Local tomography: volcanoes and the accretionary plate boundary in Iceland*, pp. 116–134, Chapman and Hall, London.
- Gandino, A., Guidi, M., Merlo, C., Mete, L., Rossi, R., Zan, L. (1985), Preliminary model of the Ribeira Grande geothermal field (Azores Islands), *Geothermics*, 14, 91–105.
- Gongora, E., Carrilho, F., Oliveira, C. (2004), Calibration of local magnitude M_L in the Azores archipelago based on recent digital recordings, *Pure Appl. Geophys.*, 161, 647–659.
- Guest, J. E., Gaspar, J. L., Cole, P. D., Queiroz, G., Duncan, A. M., Wallenstein, N., Ferreira, T., Pacheco, J. M. (1999), Volcanic geology of Furnas Volcano, São Miguel, Azores, *J. Volcan. Geotherm. Res.*, 92, 1–29.
- Hansen, S., Thurber, C., Mandernach, M., Haslinger, F., Doran, C. (2004), Seismic Velocity and Attenuation Structure of the East Rift Zone and South Flank of Kilauea Volcano, Hawaii, *Bull. Seism. Soc. Am.*, 94, 1430–1440.
- Humphreys, E., Clayton, R. W. (1988), Adaptation of back projection tomography to seismic travel time problems, *J. Geophys. Res.*, 93, 1073–1085.
- Husen, S., Smith, R. B., Waite, G. P. (2004), Evidence for gas and magmatic sources beneath the Yellowstone volcanic field from seismic tomography imaging, *J. Volcan. Geotherm. Res.*, 131, 397–410.
- Jónsson, S., Alves, M. M., Sigmundsson, F. (1999), Low rates of deformation of the Furnas and Fogo Volcanoes, São Miguel, Azores, observed with the Global Positioning System, 1993–1997, *J. Volcan. Geotherm. Res.*, 92, 83–94.
- Julian, B. R., Ross, A., Foulger, G. R., Evans, J. R. (1996), Three-dimensional seismic image of a geothermal reservoir: The Geysers, California, *Geophys. Res. Lett.*, 23,

685–688.

Kissling, E., Ellsworth, W. L., Eberhart-Phillips, D., Kradolfer, U. (1994), Initial reference models in local earthquake tomography, *J. Geophys. Res.*, 99, 19635–19646.

Lees, J. M., Crosson, R. S. (1989), Tomographic inversion for three-dimensional velocity structure at Mount St. Helens using earthquake data, *J. Geophys. Res.*, 94, 5716–5728.

Leveque, J. J., Rivera, L., Wittlinger, G. (1993), On the use of the checkerboard test to assess the resolution of tomographic inversion, *Geophys. J. Int.*, 115, 313–318.

Lomax, A. J., Virieux, J., Volant, P., Berge, C. (2000), Probabilistic earthquake location in 3D and layered models: Introduction of a Metropolis-Gibbs method and comparison with linear locations, in *Advances in Seismic Event Location*, edited by C. Thurber and N. Rabinowitz, pp. 101–134, Kluwer, Amsterdam.

Londoño, J. M., Sudo, Y. (2002), Velocity structure and seismic model for Nevado del Ruiz volcano (Colombia), *J. Volcan. Geotherm. Res.*, 119, 61–87.

Lourenço, N., Miranda, J. M., Luis, J. F., Ribeiro, A., Victor, L. A. M., Madeira, J., Needham, H. D. (1998), Morpho-tectonic analysis of the Azores Volcanic Plateau from a new bathymetric compilation of the area, *Mar. Geophys. Res.*, 20, 141–156.

Luis, J. (2006), A little insight over the recent S. Miguel seismic activity, <http://w3.ualg.pt/~jluis/SMiguel.seismicity.htm>, Universidade do Algarve.

Madeira, J., Ribeiro, A. (1990), Geodynamic models for the Azores triple junction: A contribution from tectonics, *Tectonophysics*, 184, 405–415.

Masturyono, McCaffrey, R., Wark, D. A., Roecker, S. W., Fauzi, Ibrahim, G., Suckhyar (2001), Distribution of magma beneath the Toba caldera complex, north Sumatra, Indonesia, constrained by three-dimensional P wave velocities, seismicity and gravity

- data), *Geochem. Geophys. Geosyst.*, 2, 2000GC000096.
- Mavko, G. M. (1980), Velocity and attenuation in partially molten rocks, *J. Geophys. Res.*, 85, 5173–5189.
- Molina, I., Kumagai, H., LePennec, J. L., Hall, M. (2005), Three-dimensional P-wave velocity structure of Tungurahua volcano, Ecuador, *J. Volcan. Geotherm. Res.*, 147, 144–156.
- Montesinos, F. G., Camacho, A. G., Vieira, R. (1999), Analysis of gravimetric anomalies in Furnas caldera, (São Miguel, Azores), *J. Volcan. Geotherm. Res.*, 92, 67–81.
- Moore, J. N., Norman, D. I., Kennedy, B. M. (2001), Fluid inclusions gas composition from an active magmatic hydrothermal system: a case study of The Geysers geothermal field, USA, *Chemical Geology*, 173, 3–30.
- Muecke, G. K., Ade-Hall, J. M., Aumento, F., MacDonald, A., Reynolds, P. H., Hyndman, R. D., Quintino, J., Opdyke, N., Lowrie, W. (1974), Deep drilling in an active geothermal area in the Azores, *Nature*, 252, 281–284.
- Nakajima, J., Hasegawa, A. (2003), Tomographic imaging of seismic velocity structure in and around Onikobe volcanic area, Northeastern Japan: implication for fluid distribution, *J. Volcan. Geotherm. Res.*, 127, 1–18.
- Nicholson, C., Simpson, D. W. (1985), Changes in V_p/V_s with depth: implications for appropriate velocity models, improved earthquakes locations and material properties of the upper crust, *BSSA*, 75, 1105–1123.
- Ohmi, S., Lees, J. M. (1995), Three-dimensional P- and S-wave velocity structure below Unzen volcano, *J. Volcan. Geotherm. Res.*, 65, 1–26.

- Patané, D., Chiarabba, C., Cocina, O., De Gori, P., Moretti, M., Boschi, E. (2002), Tomographic images and 3D earthquake locations of the seismic swarm preceding the 2001 Mt. Etna eruption: Evidence for a dyke intrusion, *Geophys. Res. Lett.*, 29, 1497, doi:10.1029/2001GL014391.
- Patané, D., Barberi, G., Cocina, O., De Gori, P., Chiarabba, C. (2006), Time-resolved seismic tomography detects magma intrusions at Mount Etna, *Science*, 313, 821–823.
- Podvin, P., Lecomte, I. (1991), Finite difference computation of traveltimes in very contrasted velocity models: A massively parallel approach and its associated tools, *Geophys. J. Int.*, 105, 271–284.
- Ritsema, J., Allen, R. M. (2003), The elusive mantle plume, *Earth Planet. Sci. Lett.*, 207, 1–12.
- Saccorotti, G., Wallenstein, N., Ibáñez, J. M., Bonagura, M. T., Damiano, N., La Rocca, M., Quadrio, A., Silva, R., Zandomenighi, D. (2004), A seismic field survey at Fogo-Furnas volcanoes, São Miguel, Azores, *Geophysical Research Abstracts*, 6, 04493.
- Sanders, C. O., Ponko, S. C., Nixon, L. D., Schwartz, E. A. (1995), Seismological evidence for magmatic and hydrothermal structure in Long Valley caldera from local earthquake attenuation and velocity tomography, *J. Geophys. Res.*, 100, 8311–8326.
- Scarpa, R., Tronca, F., Bianco, F., Pezzo, E. D. (2002), High resolution velocity structure beneath Mount Vesuvius from seismic array data, *Geophys. Res. Lett.*, 29, 2040, doi: 10.1029/2002GL015576.
- Senos, M. L., Costa-Nunes, J. (1979), Estudo da crosta nas ilhas de S. Miguel e Terceira. Resultados preliminares, *Tech. rep.*, Instituto de Meteorologia e Geofisica, Lisboa.

- Sherburn, S., Bannister, S., Bibby, H. (2003), Seismic velocity structure of the central Taupo Volcanic Zone, New Zealand, from local earthquakes tomography, *J. Volcan. Geotherm. Res.*, 122, 69–88.
- Sigmundsson, F., Tryggvason, E. (1995), Slow inflation of the Furnas volcano, São Miguel, Azores, suggested from initial leveling and Global Positioning System measurements, *Geophys. Res. Lett.*, 22(13), 1681–1684.
- Silveira, G., Stutzmann, E., Davaille, A., Montagner, J. P., Mendes-Victor, L., Sebai, A. (2006), Azores hotspot signature in the upper mantle, *J. Volcan. Geotherm. Res.*, 156, 23–34.
- Takei, Y. (2002), Effect of pore geometry on V_p/V_s : from equilibrium geometry to crack, *J. Geophys. Res.*, 107, doi:1029/2001JB00522.
- Tryggvason, A., Bergman, B. (2006), A travelttime reciprocity discrepancy in the Podvin & Lecomte *time3d* finite difference algorithm, *Geophys. J. Int.*, 165, 432–435.
- Udías, A., López Arroyo, A., Mezcuca, J. (1976), Seismotectonics of the Azores-Alboran region, *Tectonophysics*, 31, 259–289.
- Vanorio, T., Virieux, J., Capuano, P., Russo, G. (2005), Three dimensional seismic tomography from P wave and S wave microearthquake travel times and rock physics characterization of the Campi Flegrei Caldera, *J. Geophys. Res.*, 110, doi:10.1029/2004JB003102.
- Villaseñor, A., Benz, H. M., Filippi, L., De Luca, G., Scarpa, R., Patané, G., Vinciguerra, S. (1998), Three-dimensional P-wave velocity structure of Mt. Etna, Italy, *Geophys. Res. Lett.*, 25, 1975–1978.
- Wang, Z., Cates, M. E., Langan, R. T. (1998), Seismic monitoring of a CO₂ flood in a carbonate reservoir: a rock physics study, *Geophysics*, 63, 1604–1617.

- Wu, H., Lees, J. M. (1999), Three-dimensional p and s wave velocity structures of the Coso geothermal area, California, from microseismic travel time data, *J. Geophys. Res.*, 104, 13217–13233.
- Yamawaki, T., Tanaka, S., Ueki, S., Hamaguchi, H., Nakamichi, H., Nishimura, T., Oikawa, J., Tsutsui, T., Nishi, K., Shimizu, H., Yamaguchi, S., Miyamachi, H., Yamamoto, Y., Hayashi, Y. (2004), Three-dimensional P-wave velocity structure of Bandai volcano in Northeastern Japan inferred from active seismic survey, *J. Volcan. Geotherm. Res.*, 138, 267–282.
- Zhao, D., Hasegawa, A., Horiuchi, S. (1992), Tomographic imaging of P and S wave velocity structure beneath northeastern Japan, *J. Geophys. Res.*, 97, 19909–19928.
- Zollo, A., Judenherc, S., Auger, E., DAuria, L., Virieux, J., Capuano, P., Chiarabba, C., de Franco, R., Makris, J., Michelini, A., Musacchio, G. (2003), Evidence for the buried rim of Campi Flegrei caldera from 3-d active seismic imaging, *Geophys. Res. Lett.*, 30, doi:10.1029/2003GL018173.

Figure 1. (top) Regional map showing the location and main tectonic features of the Azores Archipelago. (bottom) São Miguel map with names of the most prominent regions. The box corresponds to the area selected for the study.

Figure 2. Example of raw seismograms recorded by a short period, three-component station during the Central São Miguel experiment. Starting time of record and P and S-phase arrivals are also indicated.

Figure 3. Histogram of the daily number of earthquakes recorded by the temporary network during the 2003 seismic experiment at São Miguel. In the same plot, we show magnitude-duration values (M_D) for those events.

Figure 4. P-wave velocity model used in routine network locations (light gray line, TAC Model) and 1D model derived from our data (black line, Minimum 1D Model) from 0 to 10 km depth.

Figure 5. Stations (triangles) and earthquakes (black circles) used for the 3D inversion, projected on the horizontal plane and N-S and W-E vertical planes. P-wave ray paths (gray lines) and unused earthquakes (white circles) are also indicated. Grid parameterization (dotted lines) and 100-m topography contours are represented.

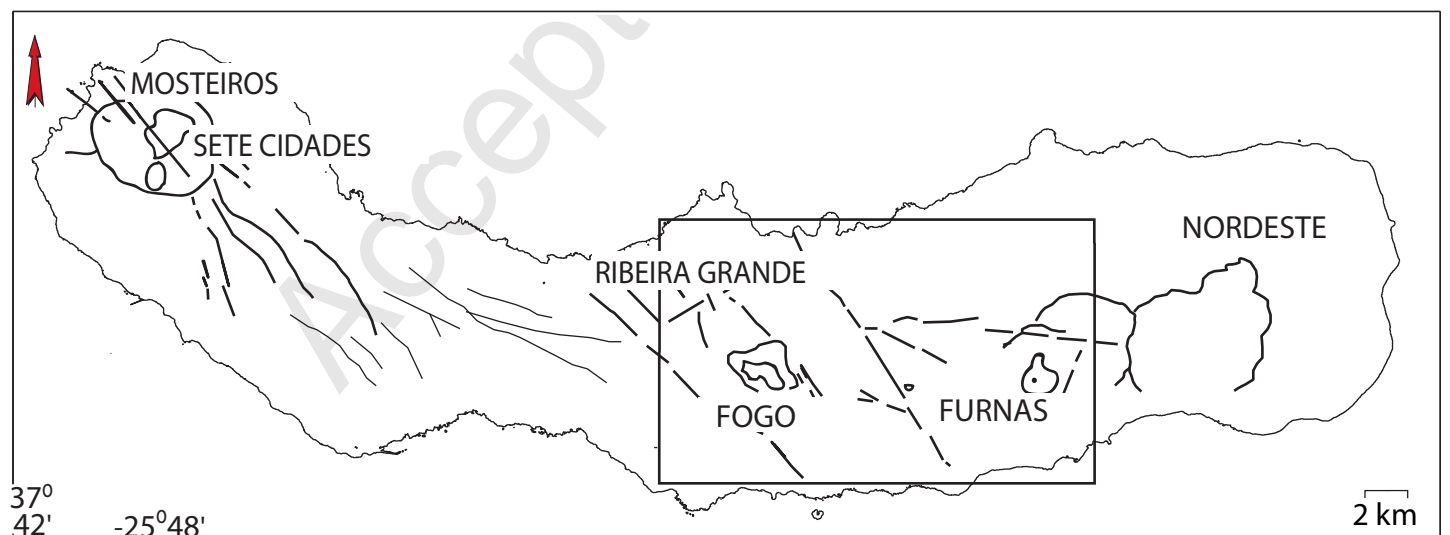
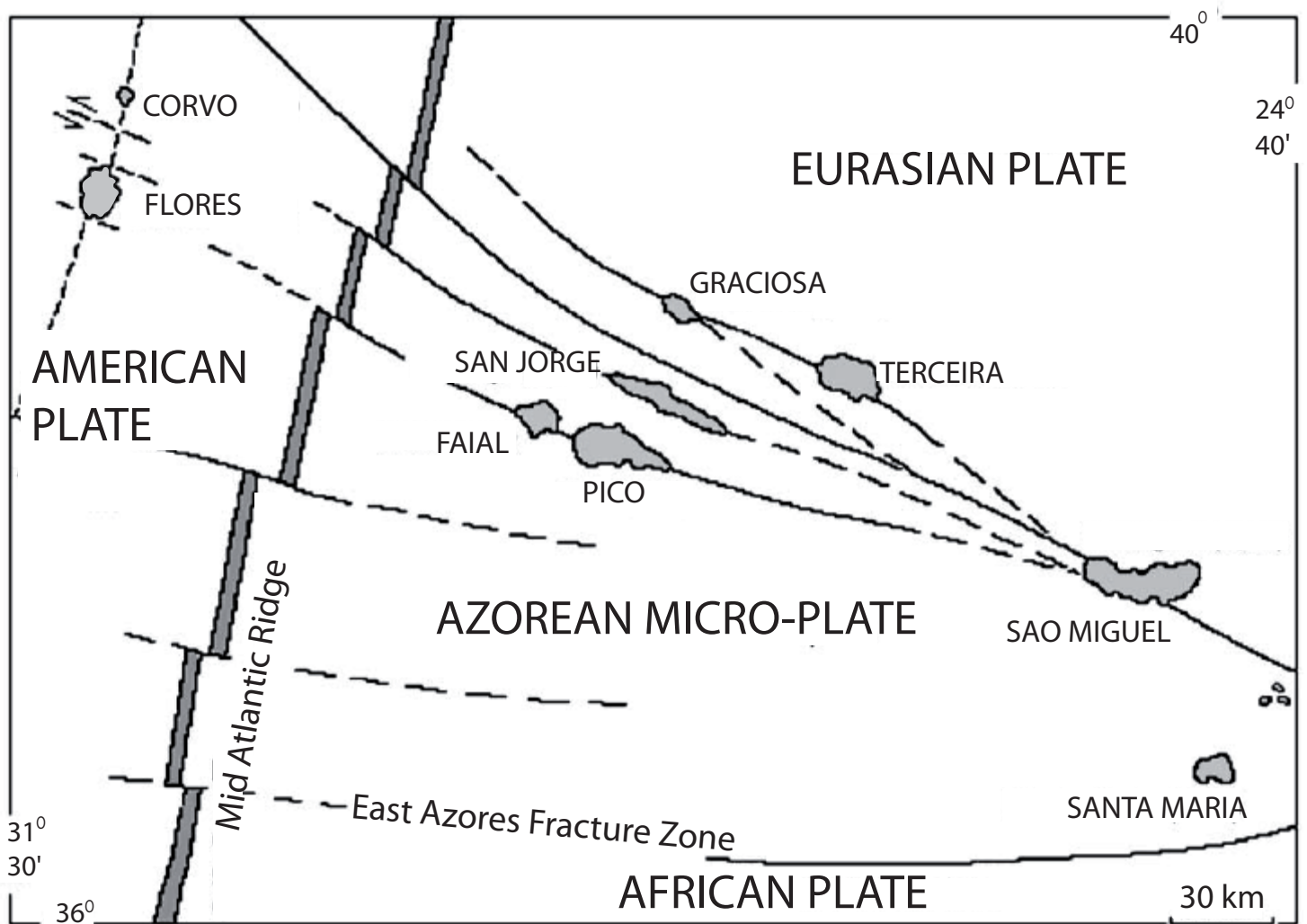
Figure 6. Distribution of final RMS and total number of used P-wave ray paths against smoothing values. The RMS is indicated in ms. The ray number is divided by 15.

Figure 7. Example of the results of a checkerboard test. Synthetic input model (left) and inverted model (right) for P-wave velocity. Map view (above) and W-E vertical section 2 km south of the map center (below). The contours indicate the total ray path length contained in each $1 \times 1 \times 1$ km cell. Contours are shown for 20 and 40 km total ray length.

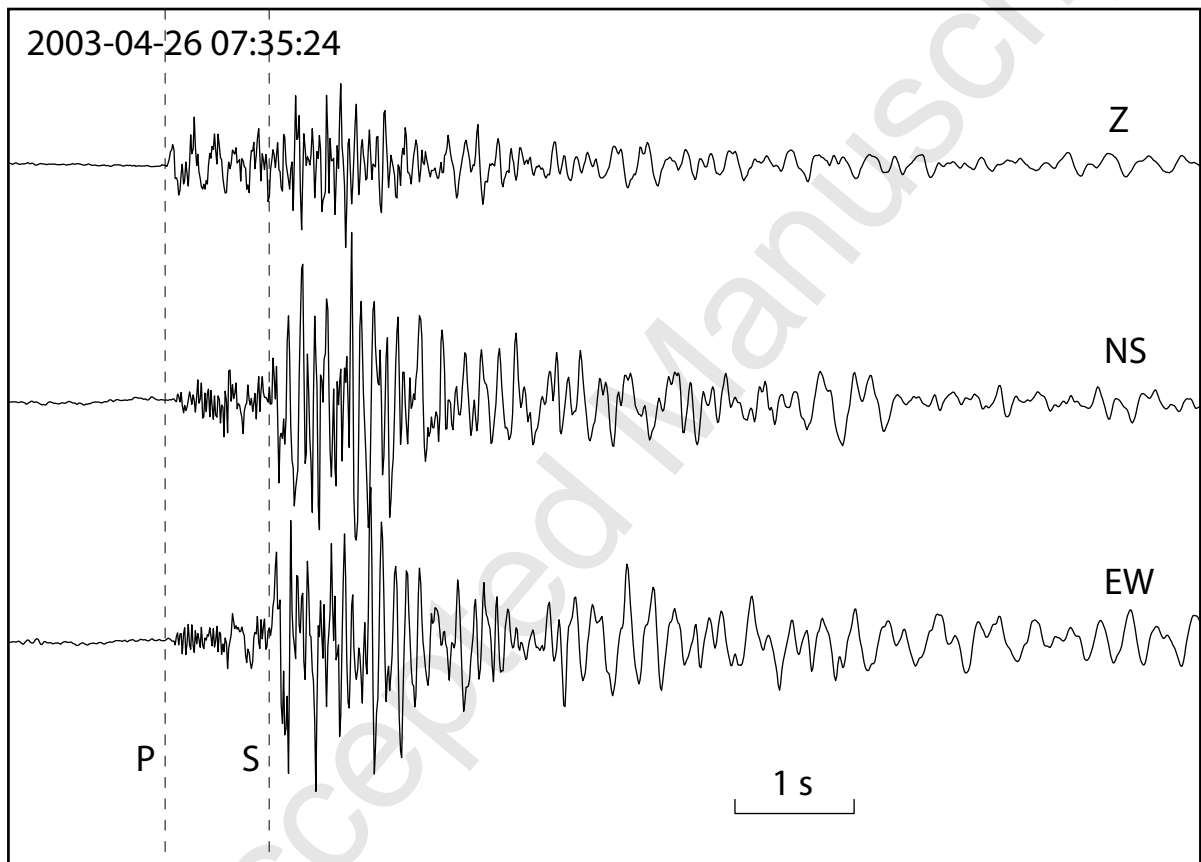
Figure 8. Example of the results of the reconstruction test. Comparison between P-wave final CSM velocity model (left) and average model from 25 different reconstruction-test inversions (right). White triangles are seismic stations. Plots are horizontal sections at 1 km depth.

Figure 9. Velocity model obtained from the tomographic inversion of P and S travel times (CSM model). (top) Topographic map of CSM with 100-m contour lines. Triangles represent seismic stations. Red symbols indicate positive (cross) and negative (circles) station residuals. Fogo and Furnas lakes are marked with a bold line. Locations of A and B vertical sections (see Figure 10) are also indicated. (left) Horizontal sections of the P-wave velocity model at different depths, in % with respect to the initial model. (right) Horizontal sections of the P- and S-wave velocity ratio. Unresolved areas are left as blank zones.

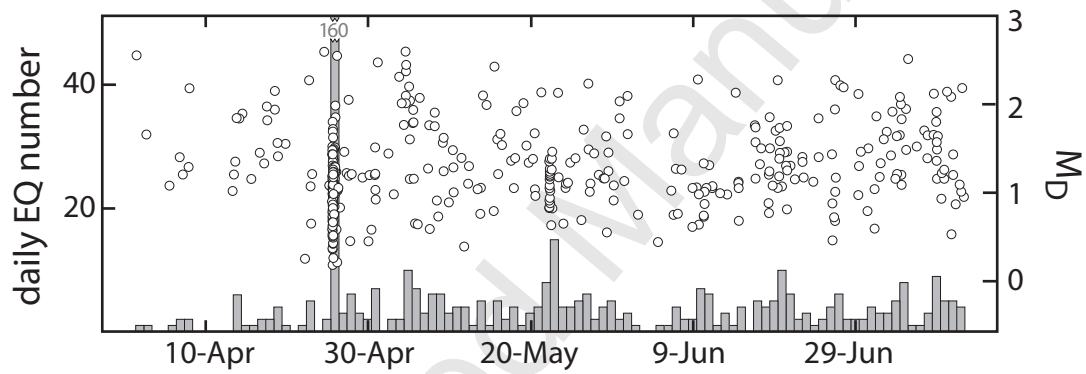
Figure 10. Vertical sections of the final model along profiles A and B (see Figure 9).



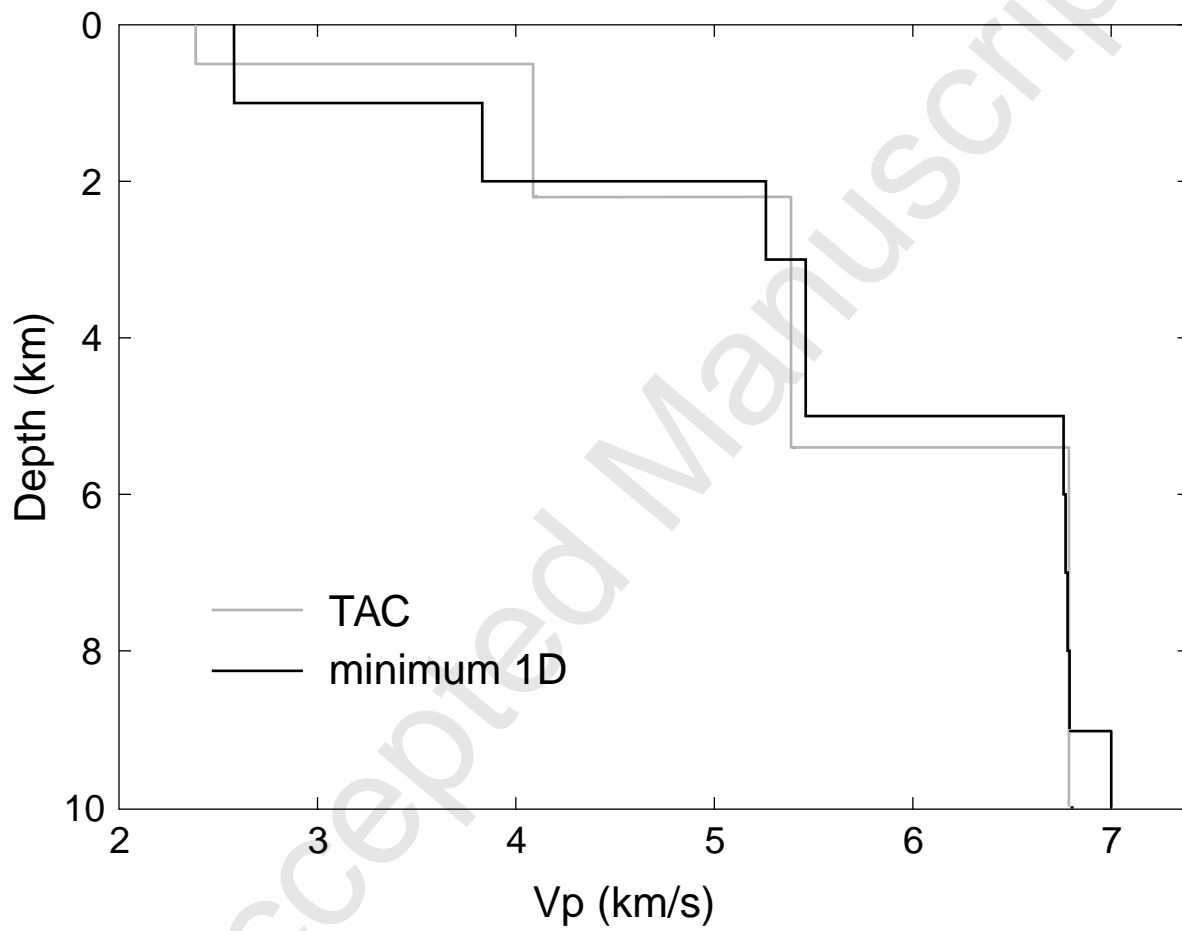
Zandomeneghi et al 2007 - Figure 1



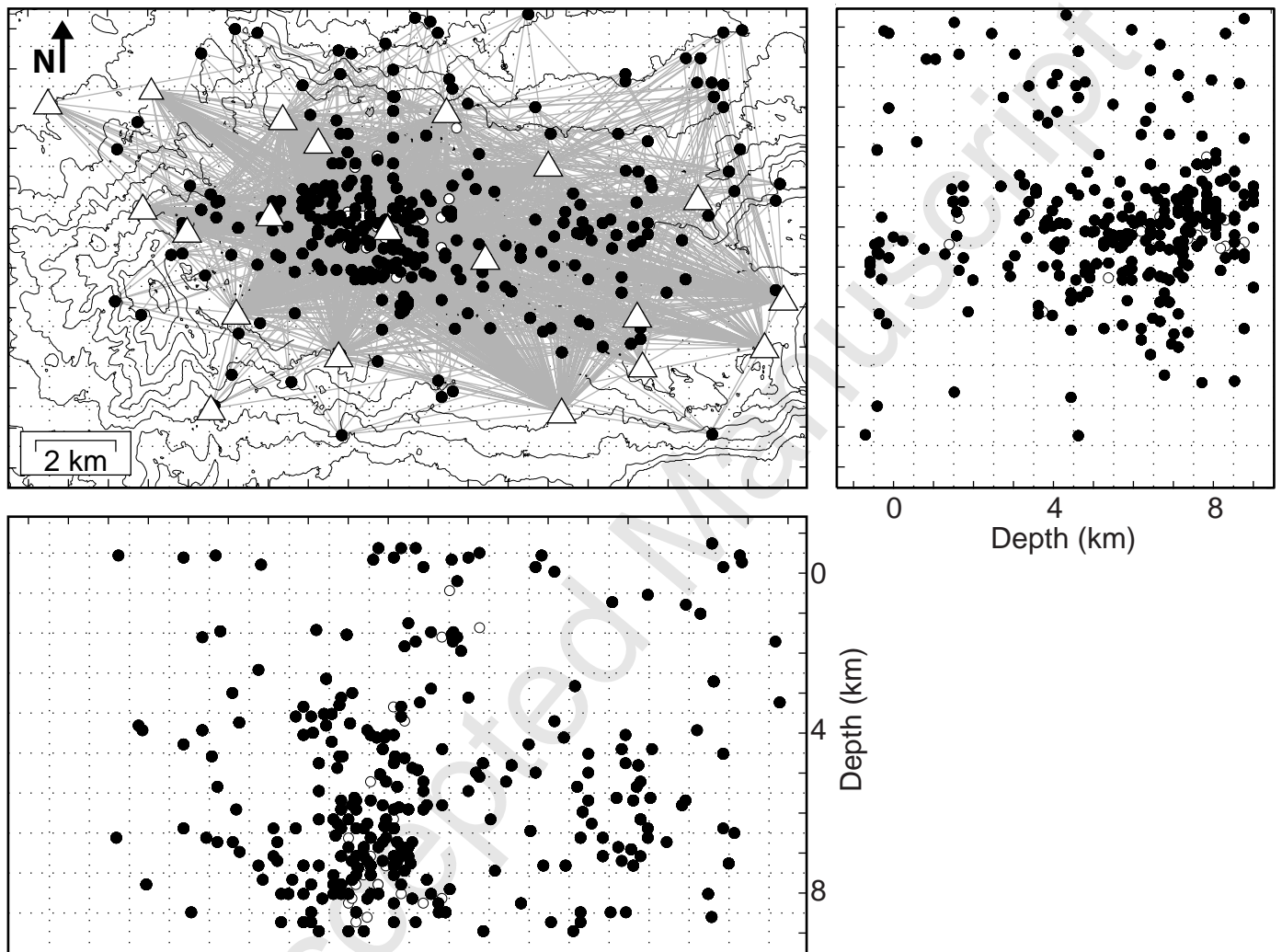
Zandomeneghi et al 2007 - Figure 2



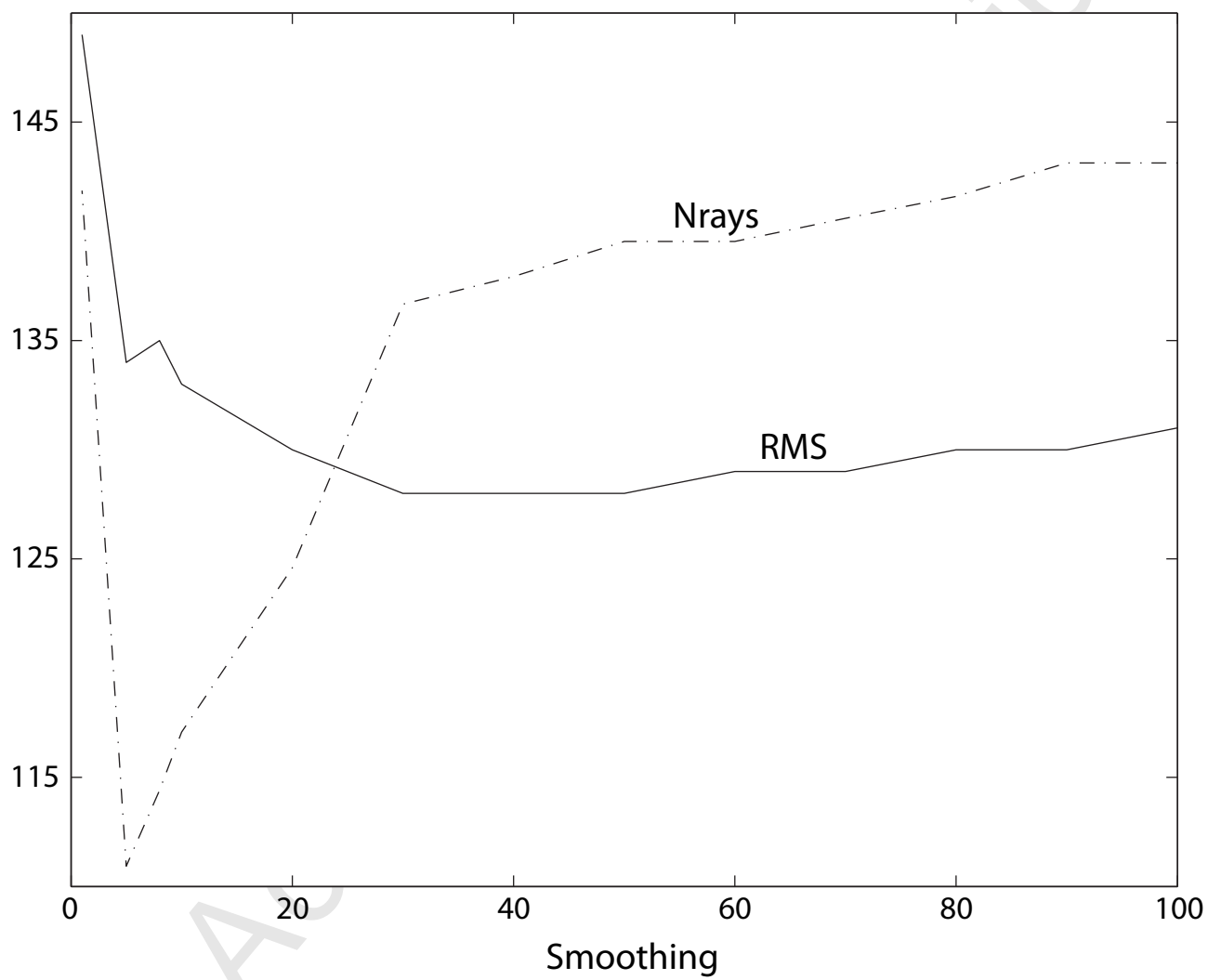
Zandomeneghi et al 2007 - Figure 3



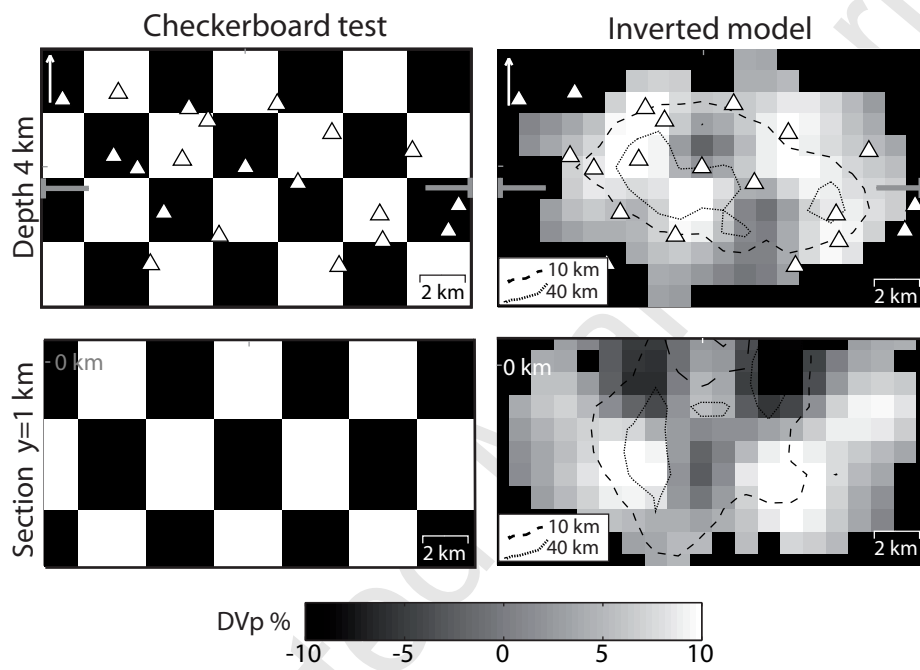
Zandomeneghi et al 2007 - Figure 4



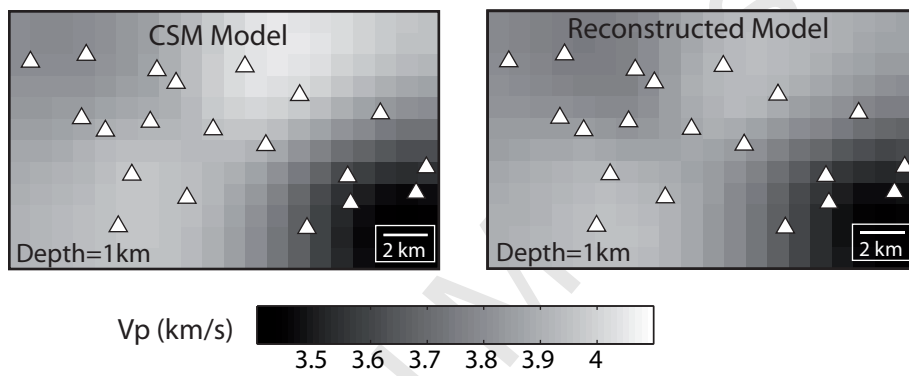
Zandomenighi et al 2007 - Figure 5



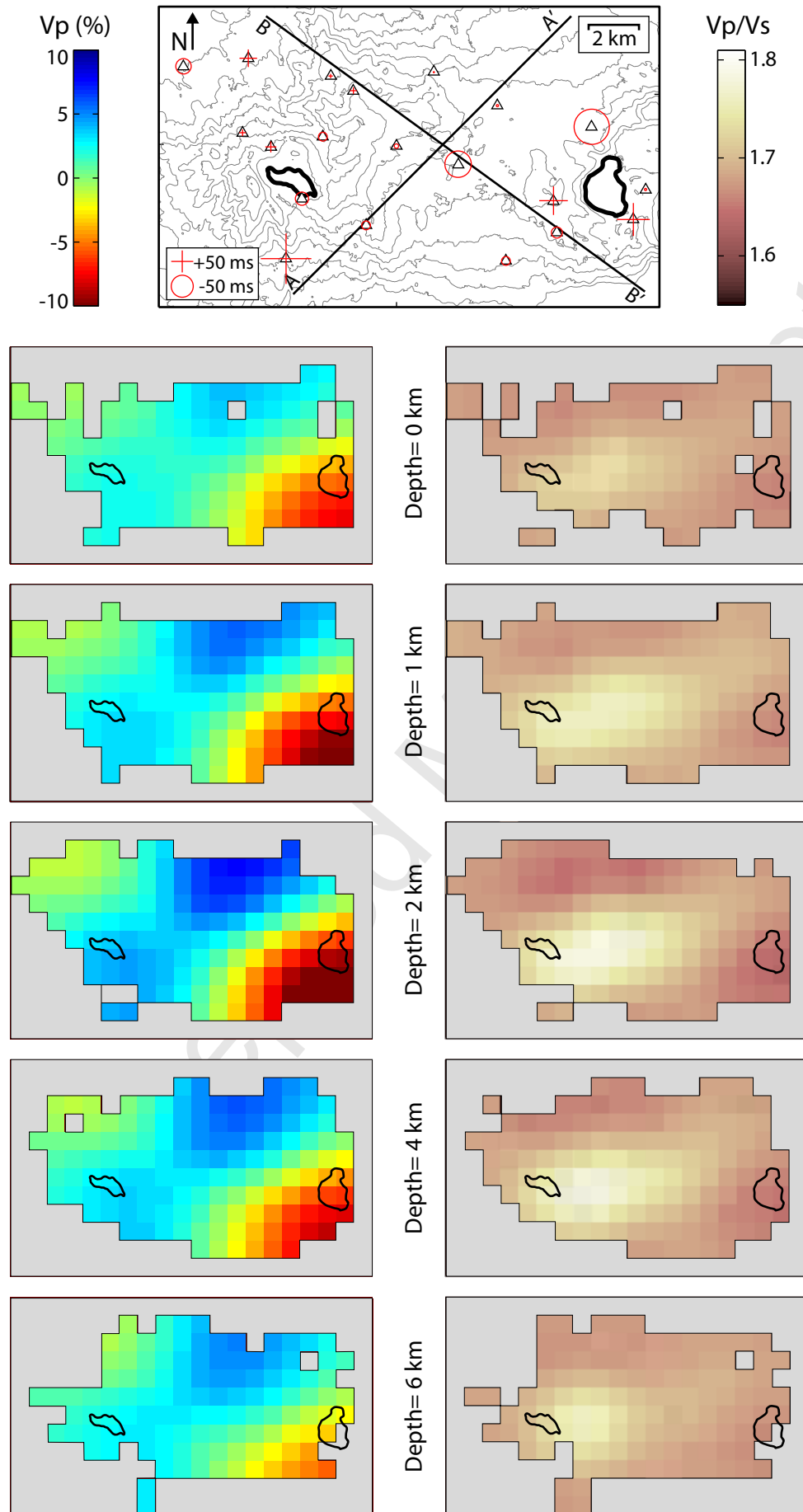
Zandomenighi et al 2007 - Figure 6



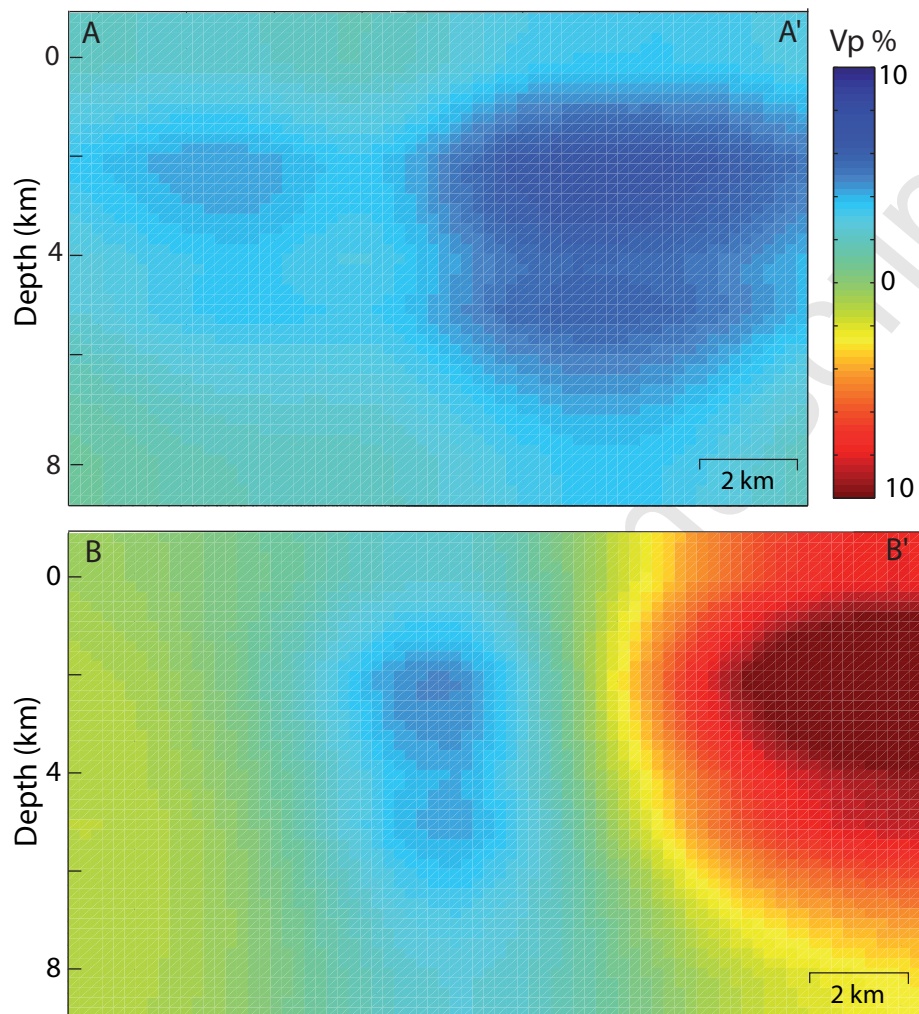
Zandomeneghi et al 2007 - Figure 7



Zandomeneghi et al 2007 - Figure 8



Zandomeneghi et al 2007 - Figure 9



Zandomeneghi et al 2007 - Figure 10